Responses of Arctic Black Carbon and Surface Temperature to Multi-Region Emission Reductions: an HTAP2 ensemble modeling study

Na Zhao[1], Xinyi Dong[2], Kan Huang[1]*, Joshua S. Fu[3,4]*, Marianne Tronstad Lund[5], Kengo Sudo[6], Daven Henze[7], Tom Kucsera[8], Yun Fat Lam[9], Mian Chin[10], Simone Tilmes[11]

[1] Shanghai Key Laboratory of Atmospheric Particle Pollution and Prevention (LAP3), Department of Environmental Science and Engineering, Fudan University, Shanghai, China

[2] School of Atmospheric Science, Nanjing University, Nanjing, China

[3] Department of Civil and Environmental Engineering, The University of Tennessee, Knoxville, Tennessee, USA.

[4] Computational Earth Science Group, Computational Sciences and Engineering Division, Oak Ridge National Laboratory, Oak Ridge, Tennessee, USA.

[5] CICERO Center for International Climate and Environmental Research, Oslo, Norway

[6] Nagoya University, Furo-cho, Chigusa-ku, Nagoya, Japan

[7] Department of Mechanical Engineering, University of Colorado, Boulder, CO, USA

[8] Universities Space Research Association, Greenbelt, MD, USA

[9] Department of Geography, The University of Hong Kong, HKSAR, China

[10] Earth Sciences Division, NASA Goddard Space Flight Center, Greenbelt, MD, USA

[11] Atmospheric Chemistry Observations and Modeling Laboratory, National Center for Atmospheric Research, Boulder, Colorado, USA

Correspondence: huangkan@fudan.edu.cn; jsfu@utk.edu

ABSTRACT

Black carbon (BC) emissions play an important role in regional climate change of the Arctic. It is necessary to pay attention to the impact of long-range transport from regions outside the Arctic as BC emissions from local sources in the Arctic were relatively small. The Task Force Hemispheric Transport of Air Pollution Phase2 (HTAP2) set up a series of simulation scenarios to investigate the response of BC in a given region to different source regions. This study investigated the responses of Arctic BC concentrations and surface temperature to 20% anthropogenic emission reductions from six regions in 2010 within the framework of HTAP2 based on ensemble modeling results. Emission reductions from East Asia (EAS) had most (monthly contributions: 0.2 - 1.5 ng m^{-3}) significant impact on the Arctic near surface BC concentrations while the monthly contributions from Europe

(EUR), Middle East (MDE), North America (NAM), Russia-Belarus-Ukraine (RBU), and South Asia (SAS) were 0.2–1.0 ng m^{-3}, 0.001–0.01 ng m^{-3}, 0.1–0.3 ng m^{-3}, 0.1–0.7 ng m^{-3}, 0.0–0.2 ng m^{-3}, respectively. The responses of the vertical profiles of the Arctic BC to the six regions were found to be different due to multiple transport pathways. Emission reductions from NAM, RBU, EUR, and EAS mainly influenced the BC concentrations in low troposphere of the Arctic, while most of the BC in the upper troposphere of the Arctic derived from SAS. The response of the Arctic BC to emission reductions of six source regions became less significant with the increase of the latitude. The benefit of BC emission reductions in terms of slowing down surface warming in the Arctic was evaluated by using Absolute Regional Temperature-change Potential (ARTP). Compared to the response of global temperature to BC emission reductions, the response of Arctic temperature was substantially more sensitive, highlighting the need for curbing global BC emissions.

1. Introduction

Black carbon (BC) is one of the short-lived climate forcers (SLCFs, AMAP, 2015) and was regarded as the second largest contributor to global warming, only inferior to carbon dioxide (Bond et al. 2013). BC over the Arctic can perturb the radiation balance in a number of ways. Direct aerosol forcing occurred through absorption or scattering of solar (shortwave) radiation. BC is the most efficient atmospheric particulate species at absorbing visible light (Bond et al., 2013), the added atmospheric heating will subsequently increase the downward longwave radiation to the surface and warm the surface (AMAP, 2011). Radiative forcing by BC can also result from aerosol-cloud interactions that affected cloud microphysical properties, albedo, extent, lifetime, and longwave emissivity (Twomey 1977; Garrett and Zhao 2006). BC has an additional forcing mechanism after depositing onto snow and ice surfaces (Clarke and Noone, 1985). The surface albedo of snow and ice could be reduced and further enhanced the absorption of solar radiation at the surface. In the Arctic, surface temperature responses were strongly linked to surface radiative forcing as the stable atmosphere of the region prevented rapid heat exchange with the upper troposphere (Hansen and Nazarenko, 2004).

The Arctic has been warming twice as rapidly as the world in the past fifty years, and has experienced significant changes in its ice and snow covers as well as permafrost (AMAP, 2017).

65 Reductions of carbon dioxide emissions are the backbone of any meaningful effort to mitigate

66 climate forcing. But even if significant reductions of carbon dioxide are made, slow down of the

67 temperature rise in the Arctic and the sea level rise caused by the melting of glaciers may not be

68 achieved in time. Hence, the goal of slowing down the deterioration of the Arctic may best be

69 achieved by also targeting at shorter-lived climate forcing agents, especially those that could impose

70 appreciable surface forcing and trigger regional-scale climate feedbacks pertaining to the melting of

71 sea ice and snow. Modelling studies by UNEP/WMO (2011) and Stohl et al. (2015) suggested that

72 the climate response of SLCFs mitigation was strongest in the Arctic region. AMAP (2011 and 2015)

73 as well as Sand et al. (2016) demonstrated that per unit of emission reductions of SLCFs in the

74 Northern areas had the largest temperature response on the Arctic, with the Nordic countries

75 (Denmark, Finland, Iceland, Norway, and Sweden) and Russia having the largest impact compared to

76 other Arctic countries such as the United States and Canada.

77   The few studies that investigated specific regional aerosol forcing (Shindell and Faluvegi, 2009;

78 Shindell et al., 2012; Teng et al., 2012) typically used a single climate model at a time to investigate

79 the climate response to idealized, historical, or projected forcing. However, different models varied

80 considerably in the representation of aerosols and radiative properties, resulting in large uncertainties

81 in simulating the aerosol radiative forcing (Myhre et al., 2013b; Shindell et al., 2013). When

82 investigating the climate response to regional emissions, such uncertainties were likely to be

83 confounded even further by the variability between models in regional climate and circulation

84 patterns and variation in the global and regional climate sensitivity (the amount of simulated

85 warming per unit radiative forcing). Hence, the Task Force Hemispheric Transport of Air pollution

86 Phase2 (HTAP2, http://www.htap.org/) incorporating multiple global models can avoid the great

87 uncertainty of single model to a certain degree, with the aim to improve model estimates of the

88 impacts of intercontinental transport of air pollutants on climate, ecosystems, and human health

89 (Galmarini et al., 2017). To date, the HTAP2 results have been explored from a variety of scientific

90 and policy-relevant perspectives. For instance, by comparing against observations, sulfur and

91 nitrogen depositions during HTAP2 had been significantly improved compared to HTAP1. From

92 2001 to 2010, the global nitrogen deposition increased 7% while the global sulfur deposition

93 decreased 3% (Tan et al., 2018a). The significant impacts of hemispheric transport on the deposition

94 were specifically focused and the deposition over the coastal regions was more sensitive to

95 hemispheric transport than the non-coastal continental regions (Tan et al., 2018b). Jonson et al. (2018)

96 assessed the contributions from different world regions to European ozone levels and contributions

97 from the non-European regions were mostly from North. America and eastern Asia, larger than those

98 from European emissions. Hogrefe et al. (2018) found that the simulated ozone over the continental

99 US varied very differently by digesting boundary conditions from four hemispheric or global models.

100 The impact of emission changes from six major source regions on global aerosol direct radiative

101 forcing was estimated (Stjern et al., 2016). In the local source regions, the radiative forcing

102 associated with SO_4^{2-} was strengthened (25%) while that from BC was weakened (37%) due to a

103 20% emission reduction. Liang et al. (2018) estimated global air-pollution-related premature

104 mortality from exposure to $PM_{2.5}$ and ozone and the interregional transport lead to more deaths

105 through changes in $PM_{2.5}$ than in O_3. However, the source region contributions to Arctic BC and the

106 spread among multi-model results have been rarely explored from the perspective of HTAP2

107 initiative.

108 This study aims to investigate the responses of Arctic BC concentrations and surface temperature

109 to 20% anthropogenic emission reductions from different regions in the Northern Hemisphere (NH).

110 A comparison of six global modeling works within the framework of HTAP2 experiments for the

111 Arctic region in 2010 was presented. The ensemble modeling results were used to apportion the

112 contribution from different source regions to the near-surface and vertical black carbon in the Arctic.

113 In addition, the Arctic surface temperature responses to the emission reductions were estimated.

114 **2. Methodology**

115 **2.1 HTAP2 experiments**

116 HTAP2 developed a harmonized emissions database covering all countries and the major sectors for

117 global and regional modeling from 2008 to 2010. The emissions database was obtained from the

118 nationally reported emissions (e.g., National Emission Inventory for the United States), the regional

119 scientific inventories (e.g., European Monitoring and Evaluation Programme (EMEP), Netherlands

120 Organisation for Applied Scientific Research (TNO) for Europe, Model Inter-Comparison Study for

121 Asia, MICS–Asia III), and the Emissions Database for Global Atmospheric Research data

122 (EDGARv4.3, emissions for South America, Africa, Russia and Oceania). Biomass burning

123   emissions were not prescribed in HTAP2. It was recommended that modeling groups used the Global

124   Fire Emissions Database (GFED4, http://globalfiredata.org/) with a temporal resolution of daily or

125   3–hour intervals. The detailed information of different regional inventories can be found in

126   Janssens–Maenhout et al. (2015).

127   Emission perturbations were conducted in sensitivity simulations to investigate the response of

128   various air pollutants in a given region to different source regions. In this study, the Arctic region was

129   the targeted receptor region of interest. Six source regions in HTAP2 experiments, namely, East Asia

130   (EAS), Europe (EUR), Middle East (MDE), North America (NAM), Russia–Belarus–Ukraine (RBU),

131   and South Asia (SAS) were selected to demonstrate their influences on the BC concentrations over

132   the Arctic region (Figure 1a). Two emission scenarios were designed for the HTAP2 simulation to

133   explore the source/receptor relationships, i.e. the base scenario (BASE) with no emission reduction,

134   and the control scenario (EASALL, EURALL, MDEALL, NAMALL, RBUALL, and SASALL)

135   with 20% reduction of all anthropogenic emissions in six regions respectively.

136
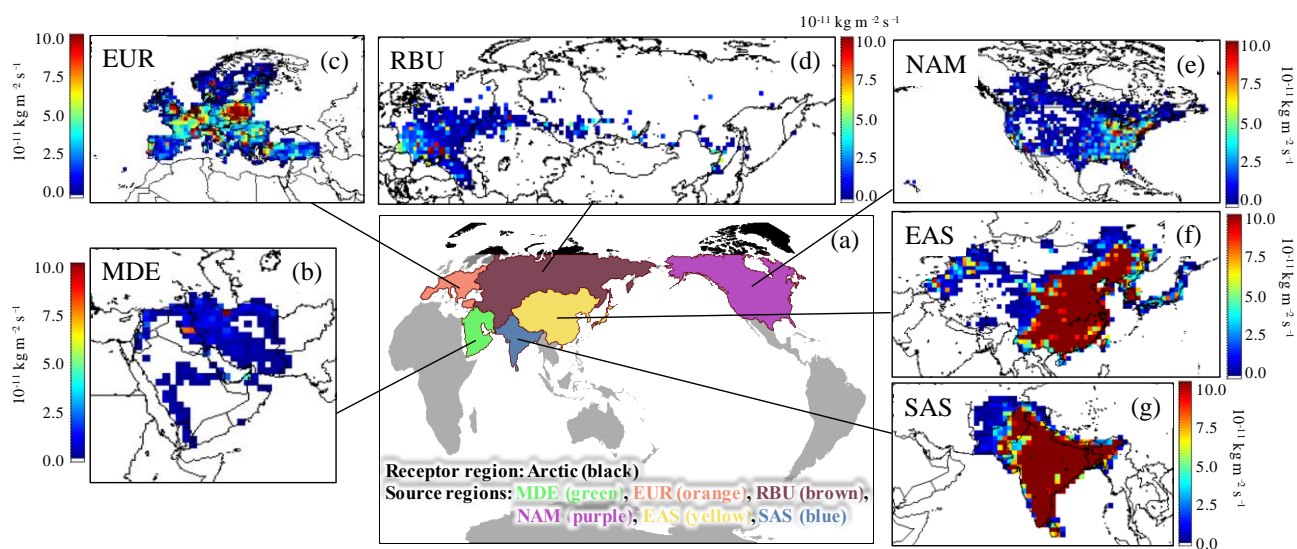
138 **Figure 1. (a)** The sketch map of receptor and source regions. **(b)–(g)** Spatial distributions of 20% reduction of
139 annual BC emission in the six source regions in 2010. MDE: Middle East; EUR: Europe; RBU:
140 Russia–Belarus–Ukraine; NAM: North America; EAS: East Asia; SAS: South Asia. The unit legends from (b) to (g)
141 are the same of 10^{-11} kg m^{-2} s^{-1}.

142 **2.1.1 Anthropogenic emission reductions of BC in HTAP2**

143   Anthropogenic BC emission sectors included power plants, industries, transportation, shipping,

144   aviation, agriculture, and residential sectors. The emission inventory had a monthly temporal

145 resolution and a spatial resolution of 0.1° × 0.1°. The total anthropogenic emissions and 20%

146 emission reductions of BC in six source regions of HTAP2 in 2010 are presented in Table 1. The

147 higher BC emission reductions were found in the EAS and SAS with the values of 355.6 and 232.5

148 Gg yr^{-1}, respectively, while were much lower in the MDE and RBU with the values of 5.3 and 18.6

149 Gg yr^{-1}, respectively. The BC emission reductions in the EAS, EUR, and RBU showed significant

150 monthly variations with higher values from November to March, while the monthly variations were

151 not obvious in the MDE, NAM, and SAS.

152

153 **Table 1.** 20% emission reductions and total anthropogenic emissions of BC in different regions of HTAP2 in 2010.

154 (Unit: Gg yr^{-1}).

Regions	Total anthropogenic emissions	20% Emission Reductions												
		Jan	Feb	Mar	Apr	May	Jun	Jul	Aug	Sep	Oct	Nov	Dec	2010
EAS[a]	1778.1	46.4	35.6	33.0	24.1	23.9	24.0	24.0	23.6	23.5	25.0	31.4	41.0	355.6
EUR[b]	326.3	6.7	6.4	7.2	6.5	5.3	4.9	4.0	3.7	4.4	5.2	5.3	5.7	65.3
MDE[c]	26.7	0.4	0.4	0.5	0.5	0.5	0.4	0.4	0.4	0.4	0.5	0.5	0.5	5.3
NAM[d]	310.8	5.2	5.1	5.3	5.1	5.1	5.2	5.3	5.3	5.1	5.1	5.1	5.2	62.2
RBU[e]	93.0	2.0	1.9	1.9	1.7	1.4	1.3	1.0	1.1	1.2	1.6	1.7	1.8	18.6
SAS[f]	1162.7	20.4	19.1	19.7	18.9	19.2	18.9	19.2	19.2	19.0	19.3	19.2	20.4	232.5
All	3697.6	81.2	68.5	67.6	56.8	55.4	54.7	53.9	53.3	53.6	56.7	63.2	74.6	739.5
Global	5492.9	110.6	86.2	92.8	103.9	98.7	97.2	86.8	85.4	85.4	84.2	83.3	83.9	1098.6

155 [a] East Asia. [b] Europe. [c] Middle East. [d] North America. [e] Russia–Belarus–Ukraine. [f] South Asia.

156 Figure 1b–g illustrates the spatial distribution of the 20% reductions of annual BC emissions in six

157 source regions in 2010. It can be found that the most intense reductions of BC emissions in EAS and

158 SAS were concentrated in East China and India, respectively, which were mainly attributed to

159 emissions from residential sectors, followed by transportation and industries. The BC emission

160 reductions of EUR were widely distributed with high values in central Europe, with residential and

161 transportation sectors accounting for the largest proportion. The reductions near the Arctic circle

162 could be found in the north of EUR, NAM, and RBU. For MDE, most BC was emitted from Iran,

163 which located in the northeast of this region. Overall, the spatial pattern of BC emission reductions in

164 six regions was closely related to the spatial distribution of the human population.

165 **2.1.2 Model description**

166 Considering that the simulations should cover all months of 2010 and all emission source regions,

167 five global models (i.e. CAMchem, CHASER_re1, GEOS-Chem, GOCART–v5, and Oslo CTM3–v2)

168 were incorporated to simulate the responses of BC concentrations in the Arctic to 20% BC emission

169 reductions from EAS, EUR, MDE, NAM, RBU, and SAS, respectively. The brief information of

170 model configurations is listed in Table 2. As required by HTAP2, all simulations should include a

171 spin-up time of 6 months prior to the period of interest. The outputs from all models are available

172 upon request from http://aerocom.met.no. The time resolution of the outputs used in this study is

173 monthly for all models, although models were run at a finer resolution (e.g., daily or hourly). The

174 model outputs for air pollutants were originally provided in the unit of mass mixing ratio (MMR, kg

175 kg^{-1}). To facilitate comparison between model and observation and further data analysis, we

176 converted the original units into ng m^{-3} based on the ideal gas law (Aamaas et al., 2017).

177

178 **Table 2.** Configurations of models used in this study

Models	Meteorological field	Horizontal resolution	Vertical layers	Convection	Reference
CAMchem	GEOS5 v5.2	$1.9° \times 2.5°$	56	Zhang–McFarlane approach for deep convection	Lamarque et al., 2012; Tilmes et al., 2016
CHASER_re1	ERA-Interim and HadISST	$2.8° \times 2.8°$	32	CCSR/NIES AGCM for advection, convection, and other subgrid–scale mixing	Sudo et al., 2002; Takashi et al., 2018
GEOS-Chem	GEOS–5 (MERRA)	$2.0° \times 2.5°$	47	Convective transport is computed from the convective mass fluxes in the meteorological archive	Henze et al., 2007
GOCART–v5	MERRA	$1.3° \times 1.0°$	72	MERRA for moist convection, Arakawa–Schubert (RAS) algorithm for GCTM	Chin et al., 2000
Oslo CTM3–v2	ECMWF–IFS	$2.8° \times 2.8°$	60	Tiedke mass flux scheme for deep convection	Søvde et al., 2012; Lund et al., 2018

179 **2.2 Calculation of the temperature response to BC emissions reduction**

180 The climate effects of air pollutants have been the focus of climate change research since the last

181 century (IPCC, 1990; IPCC, 2001). In the last few years, the metrics for estimating this kind of effect

182 have been constantly improving (Shindell et al., 2012; Bond et al., 2013; Smith and Mizrahi, 2013;

183 Stohl et al., 2015). The Intergovernmental Panel on Climate Change (IPCC) used the Global

184 Warming Potential (GWP) as a method for comparing the potential climate impact of emissions of

185   different greenhouse gases (IPCC, 1990). GWP is the time-integrated radiative forcing due to a pulse

186   emission of a given species, over some given time horizon (commonly 20, 100, or 500 years) relative

187   to a pulse emission of carbon dioxide. GWP does not purport to represent the impact of air pollutant

188   emissions on temperature. Although a short-lived climate pollutant (SLCP) could have the same

189   GWP as a long-lived climate pollutant, identical (in mass terms) pulse emissions could cause a

190   different temperature change at a given time, because long-lived climate pollutants accumulate in the

191   climate system while short-lived climate pollutants can be broken down by various processes.

192   Consequently, warming caused by long-lived climate pollutants is determined by total cumulative

193   emissions to date, while the warming due to short-lived climate pollutants is determined more by the

194   current rate of emissions in any given decade and depends much less on historical emissions. This

195   means the importance of SLCP emissions is often overstated based on GWP. Shine et al. (2005)

196   proposed the Global Temperature Change Potential (GTP) as a replacement for GWP to represent the

197   global-mean surface temperature change for both a pulse emission (GTP_P) and a sustained change in

198   emissions (GTP_S) of a given air pollutant. The distinction between GTP_P and GTP_S avoids the

199   overestimation of GWP for the short-lived climate pollutants. Even for a uniform forcing, there will

200   be differences of spatial patterns in the temperature response. Regional Temperature-change Potential

201   (RTP) (Shindell and Faluvegi, 2010) was applied to analyze the temperature response on the regional

202   scale, since both GWP and GTP focused on the global scale. The GWP, GTP, and RTP were

203   normalized to the corresponding effect of CO_2 as the Absolute Global Warming Potential (AGWP),

204   Absolute Global Temperature Change Potential (AGTP), and Absolute Regional Temperature-change

205   Potential (ARTP), respectively. AGWP represented the absolute forms of radiative forcing. AGTP

206   and ARTP represented the absolute forms of temperature perturbation.

207   ARTPs is more suitable for this study to calculate the temperature response, considering that the

208   research object is BC with short lifetime and focus on regional impact of the BC emission reductions

209   on temperature changes in the Arctic. For SLCFs with atmospheric lifetimes much shorter than both

210   the time horizon of the ARTP and the response time of the climate system, the general expression for

211   the ARTP following a pulse emission of BC (E) in region r which leads to a response in latitude band

212   m is as follows (Fuglestvedt et al., 2010; Collins et al., 2013; Aamaas et al., 2017):

213    $$ARTP_{r, m, s}(H) = \sum_l \frac{F_{l, r, s}}{E_{r, s}} \times RCS_{l, m} \times R_T(H) \qquad (1)$$

214    $F_{l,r,s}$ (in W m^{-2}) is the radiative forcing in latitude band l due to emission in region r in season s as

215   a function after the pulse emission $E_{r,s}$ (in Tg). Even though our estimates are based on seasonal

216   emissions, the temperature responses calculated are annual means. Shindell and Faluvegi (2009)

217   analyzed BC climate effect in four different latitudes: southern mid-high latitudes (90°S–28°S),

218   tropics (28°S–28°N), northern mid-latitudes (28°N–60°N), and the Arctic (60°N–90°N), which gives

219   a better estimate of the global temperature response as it accounts for varying efficacies with latitude.

220   The $RCS_{l,m}$ is a matrix of regional response coefficients based on the RTP concept (unitless; Collins

221   et al., 2013). As these response coefficients are normalized here, they contain no information on

222   climate sensitivity, only the relative regional responses in the different latitude bands. The global

223   climate sensitivity is included in the impulse response function R_T, which is a temporal temperature

224   response to an instantaneous unit pulse of RF (in K m^2 W^{-1}). This paper refers to the ARTP values in

225   Aamaas et al. (2017). Aamaas et al. (2017) applies two refinements of the forcing-response

226   coefficients for radiative forcing occurring in the Arctic: one for the aerosol effects in the atmosphere

227   (Shindell and Faluvegi, 2010; Lund et al., 2014) and another for the effects due to BC on snow

228   (Flanner, 2013). The ARTP in this study estimated of the direct effect in the Arctic included both the

229   direct radiative forcing from outside the Arctic and within the Arctic, while the ARTP of the

230   semi-direct effect in the Arctic was due to the semi-direct radiative forcing from outside the Arctic.

231   The contribution by radiative forcing within the Arctic to Arctic temperature changes considered the

232   vertical profile of BC concentrations as both $F_{Arctic,r,s}$ and $RCS_{Arctic,Arctic}$ have a dependence on the

233   height of the BC (Lund et al., 2014; Lund et al., 2017). The total response in the Arctic was the sum

234   of the contributions from BC forcing outside of the Arctic and inside of the Arctic.

235   Regional temperature responses at time t of an emission $E(t)$ can be calculated with these ARTP

236   values by a convolution (Aamaas et al., 2016). The temperature response is as follows:

237    $\Delta T_{r,\,m,s,\,t}(t) = \int_0^t E_{r,\,s,\,t}(t') \times ARTP_{r,m,s,\,t}(t-t')dt'$ (2)

238    $\Delta T_{r,m,s,t}$ refers to the decrease of the Arctic or global surface temperature after 20, 100, or 500 years

239   to 20% BC emission reductions of six regions (namely EAS, EUR, MDE, NAM, RBU, and SAS) in

240   the framework of HTAP2 either during summer or winter in this paper.

3. Results and Discussion

3.1 Model evaluation

To evaluate the model performance from all five models, the monthly simulated surface BC concentrations of the BASE scenario were compared with the observations at four monitoring sites in the Arctic Circle in 2010. The locations of the four sites, including Alert (82.5°N, 62.3°W) in Canada, Barrow (71.3°N, 156.6°W) in Alaska, Tiksi (71.59°N, 128.92°E) in Russia, and Zeppelin (78.9°N, 11.9°E) in Norway, are plotted in Figure S1 in the Supporting Information.

Metrics (Text S1) including correlative coefficient (COR), normalized mean bias (NMB), normalized mean error (NME), mean bias (MB), and mean absolute error (MAE) were selected for evaluating the model performance in this study (U.S. EPA, 2007) In addition to the evaluation for each single model, the multi-model ensemble mean (calculated as the average of all participating models) was also evaluated. The statistical results are listed in Table 3 and Table S1. A comparison between the monthly variations of simulated and observed BC concentrations is shown in Figure S2 (a).

The correlations of the simulated BC concentrations among different models were moderate to high with CORs ranging from 0.33 to 0.98 (Table S1), suggesting the temporal variations of different models were relatively consistent. Overall, CAMchem, GEOS-Chem, GOCART–v5, and Oslo CTM3–v2 underestimated the near-surface BC (Figure S2a), which may be attributed to an underestimation of BC emissions, e.g., gas flaring (Huang et al., 2014, 2015; Stohl et al., 2013) and shipping emissions (Marelle et al., 2016). Also, appropriate temporal allocation of BC emissions from residential combustion was another important factor governing the model performance (Stohl et al., 2013). However, the simulated BC surface concentrations from CHASER_re1 were higher than those of the other four models and observations (Figure S2a), which mainly due to their slow BC aging-rate in remote/polar regions (Sudo et al., 2015).

Table 3 shows the model performances at the four Arctic sites. No single model could reproduce the BC concentrations in the Arctic well, and models performed differently at different monitoring sites. Relatively good agreement between the observation and models was found at Zeppelin, with CORs, NME, MB, and MAE of 0.59–0.83, 38.59%–142.64%, –13.53–14.97 ng m^{-3}, and 5.40–14.97

269 ng m^{-3}, respectively. The best correlation (0.83) was found at Zeppelin from Oslo CTM3, while the

270 smallest NMB (38.59%) and MAE (5.40 ng m^{-3}) were found at Zeppelin from GOCART. On the

271 contrary, the simulated BC concentrations didn't agree so well with observations at the other three

272 sites with even negative COR values in some models (e.g., CAMchem, and CHASER_re1), which

273 may be explained by the uncertainties in emission inventory, the bias in the meteorological

274 simulations, and chemical mechanisms (Miao et al., 2017; Zhang et al., 2019). All models, except

275 Oslo CTM3, overestimated the BC concentrations in Barrow in July (Figure S2a), mainly due to the

276 large contributions of biomass burning from Siberia in the simulations caused by overestimations of

277 emissions and/or too little removal during transport (Sobhani et al., 2018).

278 The vertical profiles of simulated BC concentrations of the BASE simulation were also compared

279 with aircraft measurements from HIAPER Pole-to-Pole Observations (HIPPO) during 24 March–16

280 April 2010 (Figure S2b). Different from comparison between observed and simulated BC

281 concentrations near the surface, the vertical profiles of BC concentrations were overestimated by

282 most models. As the aircraft ascended and descended along each flight track, BC concentrations from

283 HIPPO varied with time, latitude, longitude, and altitude. However, most of the simulation results of

284 HTAP2 were provided in the temporal resolution of monthly, simulation and observation results

285 cannot be exactly matched. This partly explained the difference between the simulations and

286 observations. In general, the model ensemble mean could capture the vertical pattern of observed BC

287 profiles.

288 Although the single model didn't reproduce the BC concentrations in the Arctic well, the

289 consistency of the model ensemble mean with the observation was improved to some extent. The

290 NME and MAE of model ensemble mean was closer to zero compared with the single model.

291 Therefore, the multi-model ensemble mean was used for further analysis.

292

293 **Table 3** Comparison of the simulations and observations of monthly surface BC concentrations at Alert, Barrow,
294 Tiksi, and Zeppelin in 2010.

Parameters	Sites	CAMchem	CHASER_re1	GEOS-Chem	GOCART–v5	Oslo CTM3–v2	Model ensemble mean
COR[a]	Alert	–0.24	–0.22	0.35	0.20	–0.24	–0.10
	Barrow	–0.28	–0.08	0.06	0.00	0.01	–0.06
	Tiksi	–0.19	0.05	0.50	0.48	0.41	0.11
	Zeppelin	0.72	0.59	0.80	0.76	0.83	0.73

NMB[b] (%)	Alert	−86.75	115.06	−57.81	−34.31	−92.38	−9.21
	Barrow	−38.43	104.10	−38.95	−8.18	−75.58	4.37
	Tiksi	−82.03	10.31	−69.76	−67.34	−84.82	−46.79
	Zeppelin	−79.93	142.64	−45.57	−9.81	−75.98	8.63
NME[c] (%)	Alert	86.75	151.30	66.37	70.77	92.38	74.69
	Barrow	72.07	124.44	69.50	84.20	75.58	72.12
	Tiksi	82.03	64.55	70.16	68.82	84.82	60.81
	Zeppelin	79.93	142.64	45.57	38.59	75.98	42.06
MB[d] (ng m^{-3})	Alert	−29.03	11.08	−21.41	−16.07	−30.16	−12.81
	Barrow	−22.13	15.35	−19.10	−11.12	−30.40	−9.44
	Tiksi	−55.99	−17.28	−48.51	−48.16	−56.26	−40.64
	Zeppelin	−13.53	14.97	−8.19	−3.59	−12.45	−1.44
MAE[e] (ng m^{-3})	Alert	29.03	31.05	22.85	22.23	30.16	23.56
	Barrow	29.01	28.91	26.71	30.30	30.40	25.22
	Tiksi	55.99	37.06	48.60	48.49	56.26	43.73
	Zeppelin	13.53	14.97	8.19	5.40	12.45	4.95

295   [a] Correlative coefficient. [b] Normalized mean bias. [c] Normalized mean error. [d] Mean bias. [e] Mean absolute error.

296   **3.2 Near-surface BC concentrations in the Arctic**

297   Before analyzing the responses of Arctic BC to emission reductions, it is necessary to understand the

298   spatial-temporal distribution of BC concentrations in the Arctic region. In this study, months from

299   May to October were defined as summer and November to April were defined as winter due to the

300   special geographical location of the Arctic (Aamaas et al., 2017).

301   Spatial distributions of Arctic near surface BC concentrations in summer and winter simulated

302   from each model are showed in Figure S4. BC simulated by CHASER_re1 showed relatively high

303   concentrations over the whole Arctic, followed by GEOS-chem and GOCART–v5, while those

304   simulated by Oslo CTM3–v2 and CAMchem were lower. The difference of simulated BC

305   concentrations between land and ocean was more obvious in summer than that in winter, especially

306   for GEOS-chem and GOCART–v5. The mean BC concentrations from the ensemble models near the

307   surface Arctic (66–90°N) were 18.6 ng m^{-3} in summer and 16.6 ng m^{-3} in winter in 2010,

308   respectively. Figure 2 shows that the BC concentrations over the polar sea ice region in winter were

309   higher than that in summer. The coverage of the polar dome expanded more southward in winter

310   (Bozem et al., 2019; Law and Stohl, 2007), allowing more BC from lower latitudinal regions to be

311   transported into the Arctic. Turbulent exchange and deposition were reduced during winter as the

312   meteorological conditions in the Arctic were stable and dry (Bradley et al., 1992; Bozem et al., 2019;

313   Law and Stohl, 2007). In addition, BC emissions in EAS, EUR, and RBU regions showed obvious

314   monthly changes with higher emissions from November to March as mentioned earlier (Section

315   2.1.1), leading to the relatively high BC concentrations over the polar sea ice region in winter. Over

316   the terrestrial areas within the Arctic Circle, summer BC concentrations were higher than winter,

317   especially in Siberia and Alaska, which were attributed to intense BC emissions from biomass

318   burning over these areas from Jun to Aug (Figure S3).

319

(a)   (b)
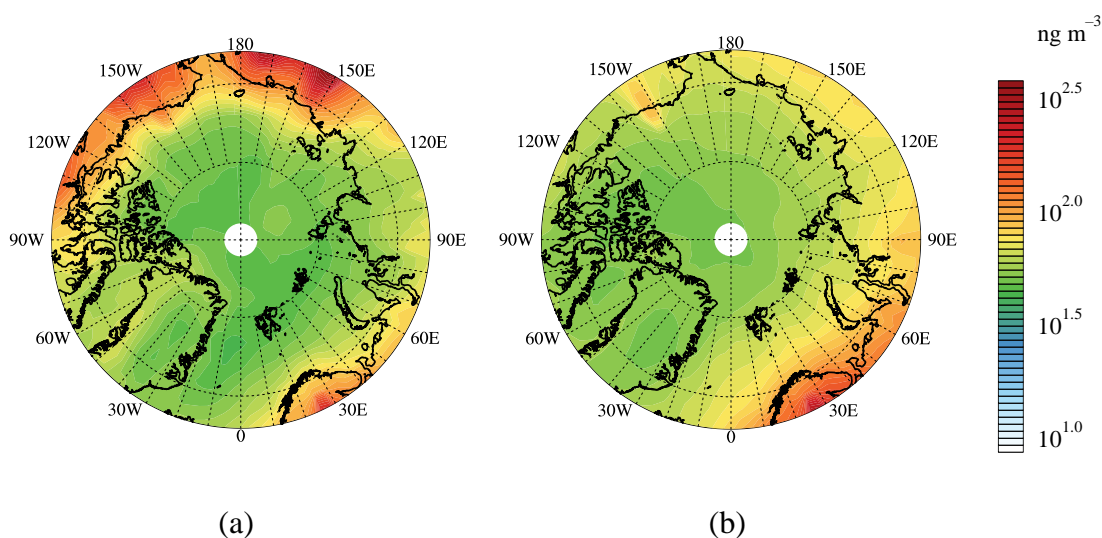
320   **Figure 2.** Spatial distribution of near-surface BC concentrations in **(a)** summer and **(b)** winter in the Arctic in 2010.

321

322   **3.3 Response of Arctic BC to 20% emission reductions**

323   **3.3.1 Contributions of regional emission reductions to the Arctic near-surface BC**

324   The response of the Arctic near-surface BC to 20% emission reductions from different source regions

325   was analyzed through emission perturbation simulations. Figure 3 shows the spatial distribution of

326   the referred response above in summer and in winter of 2010 based on multi-model ensemble mean

327   results. The source region contributions to the surface BC concentrations exhibited significant

328   seasonal variability with higher values in winter. The BC emission reductions in EAS almost affected

329   the whole Arctic, especially in winter, indicating the significance of the intercontinental transport of

330   BC. The spatial distribution of the Arctic near-surface BC response to SAS emission reductions was

331   similar to that of EAS, but the extent was much weaker. The emission reductions from EUR, NAM,

332   and RBU mainly affected the local and nearby areas, which was generally consistent with the spatial

333   pattern of emissions (Figure 1). The contribution from MDE emission reductions was very little.

334

(a₁) EASALL–summer   (a₂) EASALL–winter

(b₁) EURALL–summer   (b₂) EURALL–winter

(c₁) MDEALL–summer   (c₂) MDEALL–winter

(d₁) NAMALL–summer   (d₂) NAMALL–winter

(e₁) RBUALL–summer   (e₂) RBUALL–winter

(f₁) SASALL–summer   (f₂) SASALL–winter
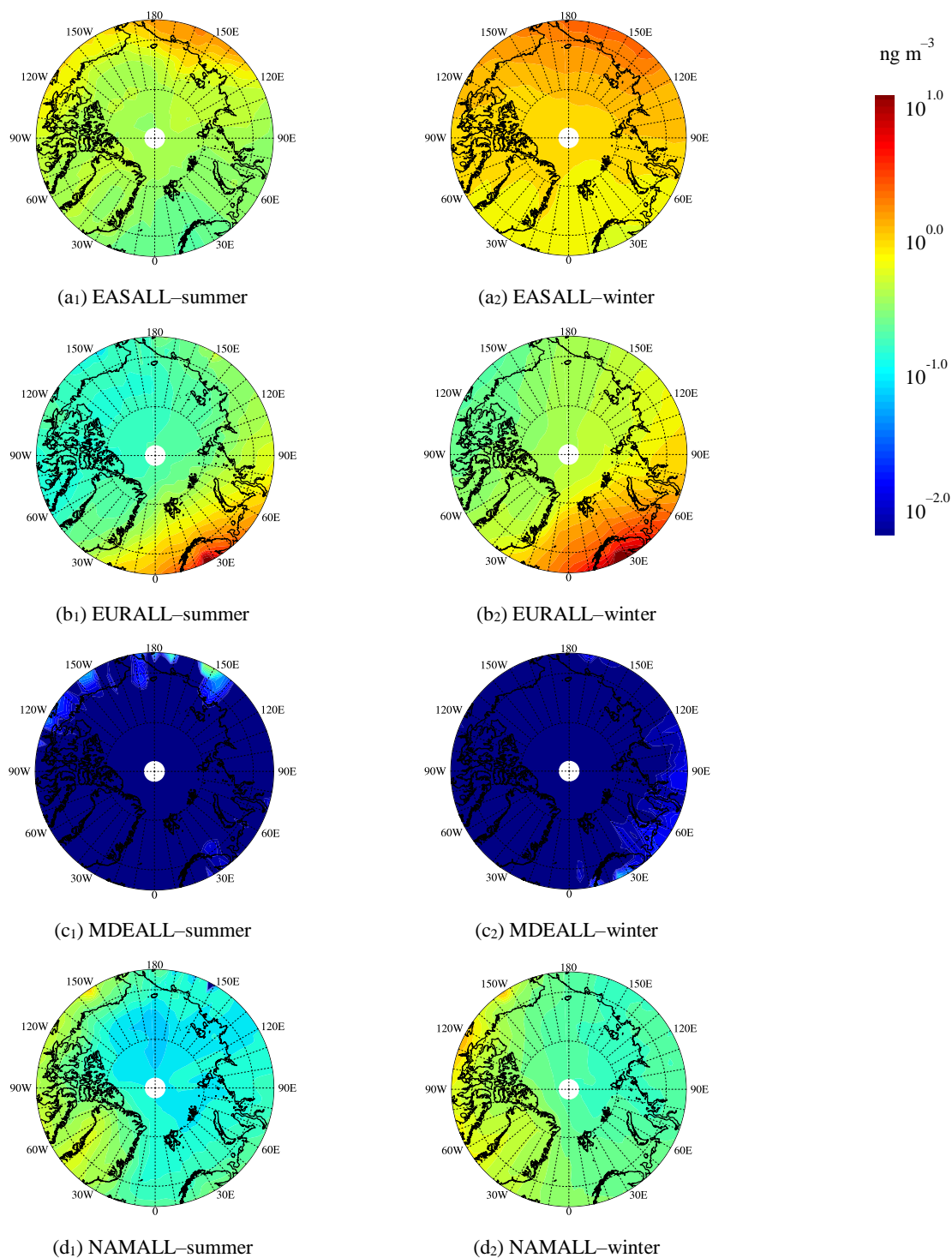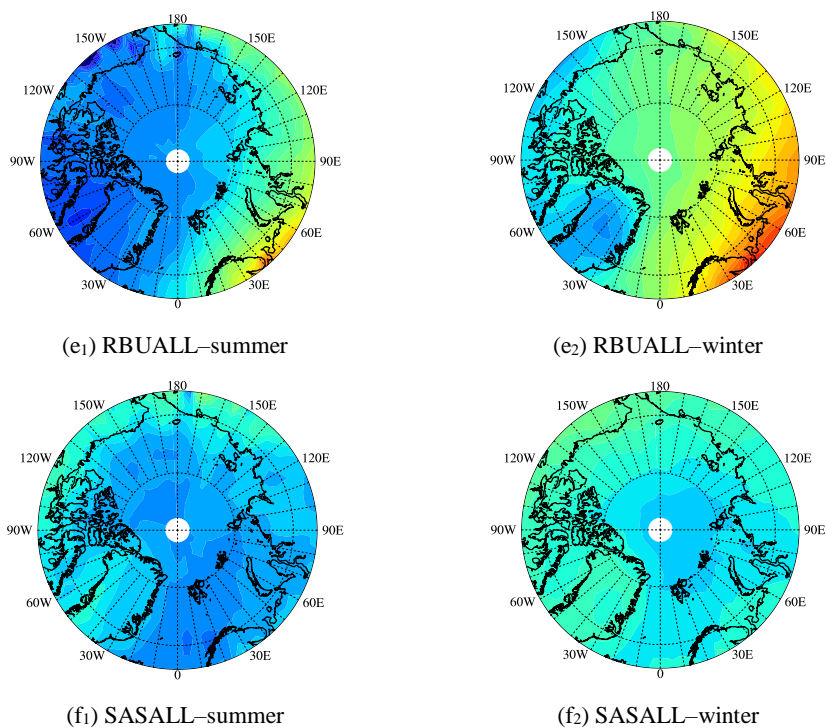
Figure 3. Spatial distribution of contribution of 20% emission reductions of different source regions to Arctic near-surface BC in summer and in winter in 2010.

The monthly variations of the response of the Arctic near-surface BC concentrations to 20% emission reductions from six source regions are presented in Figure 4. Results from the ensemble simulations are averaged over the Arctic covering latitudinal areas from 66°N to the north pole. The emission reductions from the total six source regions were 329.6 Gg during May to October, lower than that of 411.9 Gg during November to April (Table 1). Correspondingly, the contributions of 20% BC emission reductions from all six regions to Arctic near-surface BC concentrations were 0.8–1.4 ng m^{-3} during May to October and 1.5–3.2 ng m^{-3} during November to April. Arctic sensitivities (Arctic concentration change per unit source region emission change) for BC typically maximized from December to February for EUR and RBU and from March to May for EAS and NAM (Shindell et al., 2008; AMAP, 2008). The enhanced sensitivity from December to May resulted from faster transport and slower removal during winter as the meteorological conditions in the Arctic were stable and dry (Law and Stohl, 2007). The results of deposition changes also proved this result well (Figure S5). The wet deposition in summer was higher than that in winter, which was 7–13 times of dry depositions. Sharma et al. (2013) found that the Arctic region (north of 70°N) was very dry during winter with an average daily precipitation rate between 0 and 1 mm day^{-1}. Precipitation rates over some of the BC source regions such as Eurasia were at the same order of magnitude as the Arctic.

Less wet deposition and a shallow boundary layer resulted in higher BC concentrations near the surface during winter. In the summertime, the Arctic region experienced 2 to 3 times higher precipitation rates as well as wet depositions of BC relative to wintertime, thus resulting in lower contributions to the near-surface BC concentrations.

The annual contribution of 20% emission reductions from EAS, EUR, MDE, NAM, RBU, and SAS to the Arctic near-surface BC concentrations reached 0.70, 0.54, 0.01, 0.20, 0.29, and 0.09 ng m^{-3} in 2010, respectively. Correspondingly, the annual reduced column BC loadings over the Arctic were 8521.7, 2789.1, 28.8, 1762.1, 998.6, and 3640.2 ng m^{-2} in 2010, respectively.

The response of Arctic near-surface monthly BC concentration was found strongest to the 20% emission reductions from EAS with the contribution of 0.2–1.5 ng m^{-3}, accounting for 16.8%–49.0% of the total reduced BC concentrations resulting from all six source regions (Figure 4). On one hand, the BC emission reductions in EAS were the largest among the six source regions (Table 1). On the other hand, BC emission reductions in EAS can influence the Arctic lower troposphere via two pathways (Bozem et al., 2019; Stohl, 2006). BC from northern regions of EAS can enter into the polar dome of the Arctic in winter, as the air masses have cooled during transport. BC from eastern regions of EAS fast uplifted due to convection and then followed by high altitude transport in northerly directions. Radiative cooling eventually led to a slow descent into the polar dome area after air masses arrived in the high Arctic. It occurred both in summer and winter. In addition to EAS, BC emission reduction from EUR also showed significant impacts on the Arctic near-surface monthly BC concentration with the contribution of 0.2–1.0 ng m^{-3}, accounting for 20.1%–49.0% of the total reduced BC concentrations resulting from all six source regions (Figure 4). Among the three regions in the Arctic Circle (i.e. EUR, NAM, and RBU), EUR region had the largest BC emission reductions. Also, the relatively short distance between EUR and the Arctic made EUR the second most important source region to the Arctic. As for NAM and RBU, their 20% emission reductions induced moderate reductions of the monthly Arctic near-surface BC concentrations by 0.1–0.3 and 0.1–0.7 ng m^{-3}, respectively. The contribution of 20% emission reductions from SAS to the Arctic near-surface BC concentrations was much lower of 0.0–0.2 ng m^{-3} as a significant portion of BC originating from SAS accumulated in the upper troposphere (Section 3.3.2). Compared to the five source regions discussed above, the response of Arctic BC concentrations to emission reductions from MDE was negligible, owing largely to the low emissions there and long distance from the Arctic.

383
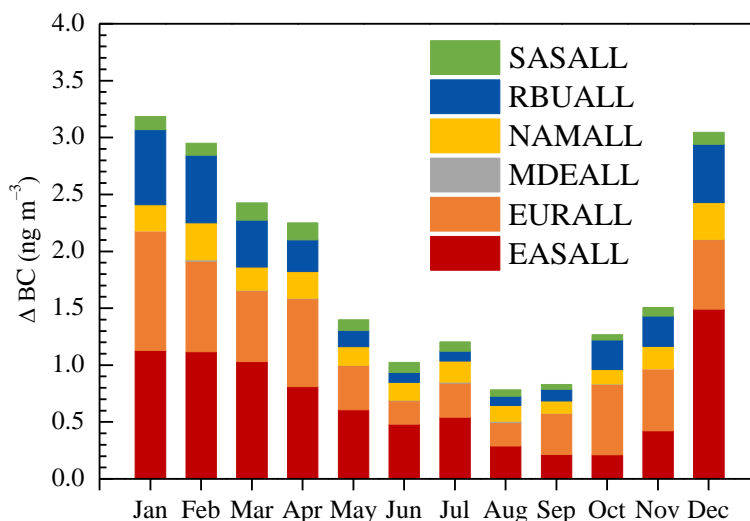
Figure 4. Monthly mean reduced concentrations of the near-surface Arctic BC due to 20% emission reductions from six source regionsin 2010.

Figure S6 compares the contributions of 20% emission reductions to Arctic near surface BC concentrations simulated by different models. All five models showed similar monthly variations, of which CHASER_re1 simulated high BC concentrations compared to the other models due to slow aging-speed (Sudo et al., 2015). All models showed the major source regions of Arctic BC from EAS, EUR, and RUB. NAM and SAS contributed moderately while the contribution from MDE was negligible.

3.3.2 Contributions of regional emission reductions to the vertical BC profiles

To assess the contributions from various source regions to the BC profiles based on the model ensemble mean, the vertical stratification needed to be unified as most participating models had different vertical settings. Since CHASER had a relatively coarse vertical resolution of 32 layers, the other models were unified to the same vertical stratification, as detailed in Table S2.

As shown in Figure 5, the contributions of regional emission reductions to BC exhibited strong vertical gradients over the Arctic. In general, the BC profiles displayed a bimodal pattern in summer, showing peaks at around 1.0–1.6 km a.s.l. (4th and 5th layers) and 8.0–8.9 km a.s.l. (13th and 14th layers). While in winter, the BC profiles showed a unimodal pattern with peaks around 0.6–1.6 km a.s.l. (3rd – 5th layers). Long-range transport of air pollutions may occur near the planetary boundary layer (Eckhardt et al., 2003; Stohl et al., 2002). High contributions in the low layers (e.g., 3rd – 5th

404   layers) were consistent with the height of the planetary boundary layer in the Arctic (Zhang, et al.,

405   2018; Cheng, 2011).

406   It has been summarized that there were several major transport pathways for BC into the Arctic

407   troposphere (Stohl, 2006). i) BC transported rapidly at low-level, followed by uplifting at the Arctic

408   front when it is located far north. Significant deposition of BC in the Arctic occurs mostly north of

409   70°N for this transport route. This transport route derived often from the high BC emission areas in

410   northern EUR but seldom from the NAM and RBU. That was mainly due to that the BC emissions

411   exist at high enough latitudes in EUR, which can be north of the polar front. However, the BC

412   emissions in NAM and RBU were concentrated south of the polar front (Figure 1), thus BC emitted

413   from these two regions can't be easily transported into the Arctic through this pathway. ii) Cold air

414   masses into the polar dome transport at low-level. This pathway derived mainly from EUR and

415   high-latitude areas of EAS during winter. The contribution of 20% emission reductions from EUR to

416   the Arctic BC concentrations peaked at around 1.0 km a.s.l. with the multi-model ensemble mean

417   value of 0.4 ng m^{-3} in summer, while peaked at lower altitude of around 1.6 km a.s.l. with the value

418   of 0.8 ng m^{-3} in winter. iii) BC could also ascend south of the Arctic followed either by high–altitude

419   transport or by several cycles of upward and downward transport, and finally slowly descended into

420   the polar dome due to radiative cooling. This was the frequent transport route from source regions

421   such as NAM, RBU, and east EAS. The contribution from NAM and RBU to the Arctic BC peaked

422   at about 1.6 km a.s.l. (0.2 ng m^{-3}) and 1.0 km a.s.l. (0.2 ng m^{-3}) in summer, and peaked at about 1.0

423   km a.s.l. (0.3 ng m^{-3}) and 0.4 km a.s.l. (0.5 ng m^{-3}) in winter. The contribution from EAS including

424   pathways ii and iii, to the Arctic BC peaked at about 1.6 km a.s.l. (0.6 ng m^{-3}) in summer and peaked

425   at about 2.4 km a.s.l. (1.6 ng m^{-3}) in winter. The contribution from MDE was negligible.

426   As shown in Figure 5, BC can also be transported into the upper troposphere of the Arctic. Air

427   masses preferably kept their potential temperature almost constant during transport as the

428   atmospheric circulation can be well described by adiabatic motions in the absence of diabatic

429   processes related to clouds, radiation, and turbulence. The potential temperature was low within the

430   polar dome area, and thus only air masses experienced diabatic cooling were able to enter the polar

431   dome (Stohl, 2006). That is to say, the air masses from SAS and low-latitude regions of EAS were

432   not easy to penetrate the polar dome but can be lifted and transported to the Arctic in the middle and

433   upper troposphere along the isentropes (AMAP, 2011; Barrie, 1986; Law and Stohl, 2007; Stohl,

434 2006). This agreed well with the previous study of Koch and Hansen (2005) and Stohl (2006). The

435 contribution from SAS to the Arctic BC concentrations peaked at about 9.7 km a.s.l. (0.4 ng m^{-3}) in

436 summer and 9.7 km a.s.l. (0.5 ng m^{-3}) winter. This was also consistent with the vertical profiles of

437 BC shown in Stjern et al. (2016). The polar dome boundary was variable in time and space and was

438 not zonally symmetric. The range of polar dome expanded southward to about 40°N over Eurasia in

439 winter as the temperature difference of different latitudes became smaller (Bozem et al., 2019; Law

440 and Stohl, 2007), resulting in the contribution of EAS to the Arctic BC concentrations in upper

441 troposphere only peak in summer at 13th layer (8.0 km a.s.l.) with the value of 0.6 ng m^{-3}.

442

(a)   (b)
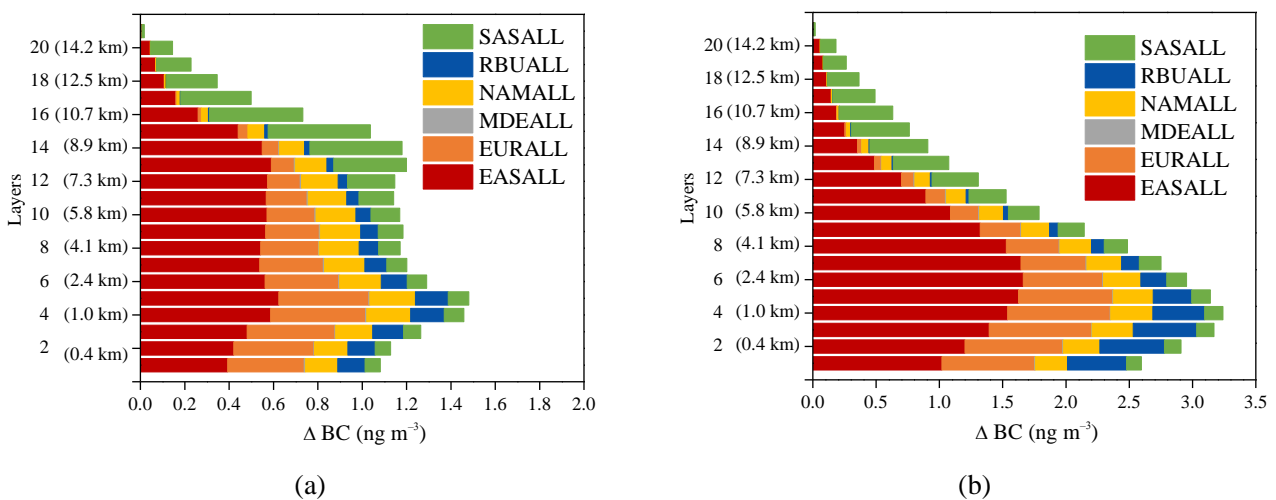
443 **Figure 5.** Contribution of 20% emission reductions from six source regions to BC concentrations in different
444 vertical layers **(a)** in summer and **(b)** in winter in the Arctic in 2010.

445 **3.3.3 Contributions of emission reductions to BC in different latitudinal bands**

446 To further analyze the response of the Arctic BC concentrations to emission reductions of six source

447 regions in HTAP2, the contribution of 20% emission reductions to BC concentrations at different

448 latitudes of the Arctic were calculated (Figures 6 and 7). In regard to the different horizontal

449 resolution of participating models, the Arctic region (66–90°N) was divided into eight latitudinal

450 bands with a 3–degree interval, which was based on the coarsest resolution of all models.

451   The response of the Arctic BC concentrations to emission reductions of six source regions became

452 weaker with the increase of the latitude due to the continuous loss of BC during transport (e.g., dry

453 and wet depositions) (Figure 6). The difference of contributions between two adjacent latitudinal

454 bands became smaller as closer to the north pole. The contributions of 20% emission reductions to

the Arctic BC concentrations near surface were the highest between 66–69°N both in summer (1.9 ng m^{-3}) and winter (4.1 ng m^{-3}), which were 1.4–2.8 times higher than the other latitudinal bands.

The contributions from EAS and EUR were higher than those from the other four regions in each latitudinal band. In detail, the contributions from EUR (0.8 ng m^{-3} in summer and 1.5 ng m^{-3} in winter) were higher than those from EAS (0.6 ng m^{-3} in summer and 1.2 ng m^{-3} in winter) in the latitudinal band of 66–69°N as the BC concentrations near surface there were more sensitive to the local emission sources. In contrast, the contributions from EAS (0.3–0.4 ng m^{-3} in summer and 0.9–1.1 ng m^{-3} in winter) were higher than those from EUR (0.2–0.4 ng m^{-3} in summer and 0.4–0.9 ng m^{-3} in winter) in the other high latitudinal bands where long-range transport played the dominant role.

The downward trends of the response of the Arctic near surface BC to emission reductions with the increase of latitude from EUR and RBU were more obvious than that of other regions (Figure 6). Dry and wet depositions of BC decreased with the increase of transport distance, and the decreasing rates became slower (Figure S7). The changes of dry and wet depositions caused by emission reductions from EUR and RBU were still obvious in the Arctic region (66°N–90°N), while depositions caused by emission reductions from the other regions tended to be gentle (Figure S7). This explains why the contribution from EAS to BC at different latitudes remained almost constant while that from EUR and RBU decreased obviously from lower latitudes to the Arctic pol
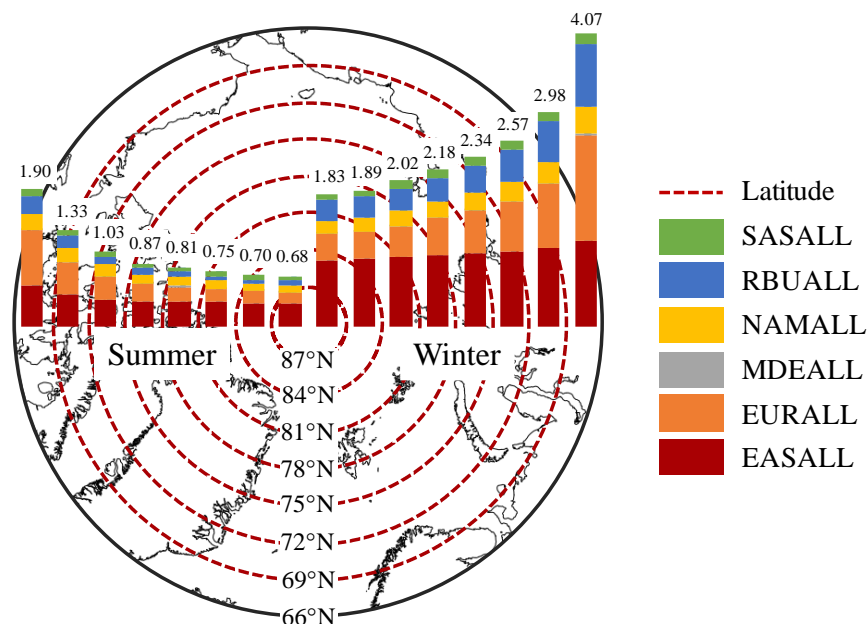
Figure 7 further depicts the response of the vertical Arctic BC profiles in different latitudinal bands to 20% emission reductions. The contributions of eight latitudinal bands showed a typical bimodal pattern in summer with peaks at 0.6–1.6 km a.s.l. (3rd – 5th layers) and 8.0–8.9 km a.s.l. (13th and 14th layers), while the contribution displayed a single peak at the 0.4–1.0 km a.s.l. (2nd – 4th layers) in winter. Similar to section 3.3.2, the peak value of the contribution at the low layers was due to the transport of EAS, EUR, NAM, and RBU emission reductions to the Arctic through different pathways both in summer and winter. The peak value in the high layers in summer was due to the transport of EAS and SAS. However, a high contribution of 20% emission reductions to BC concentrations in SAS was found in the high layers, while the contribution was low in other regions, leading to a single peak in winter. The statistical results of SAS indicated that the contribution in vertical appeared one peak at the 15th layer (9.7 km a.s.l.) with a value of 0.45–0.48 ng m^{-3} in summer and winter (Figure S8).

(a)

(b)
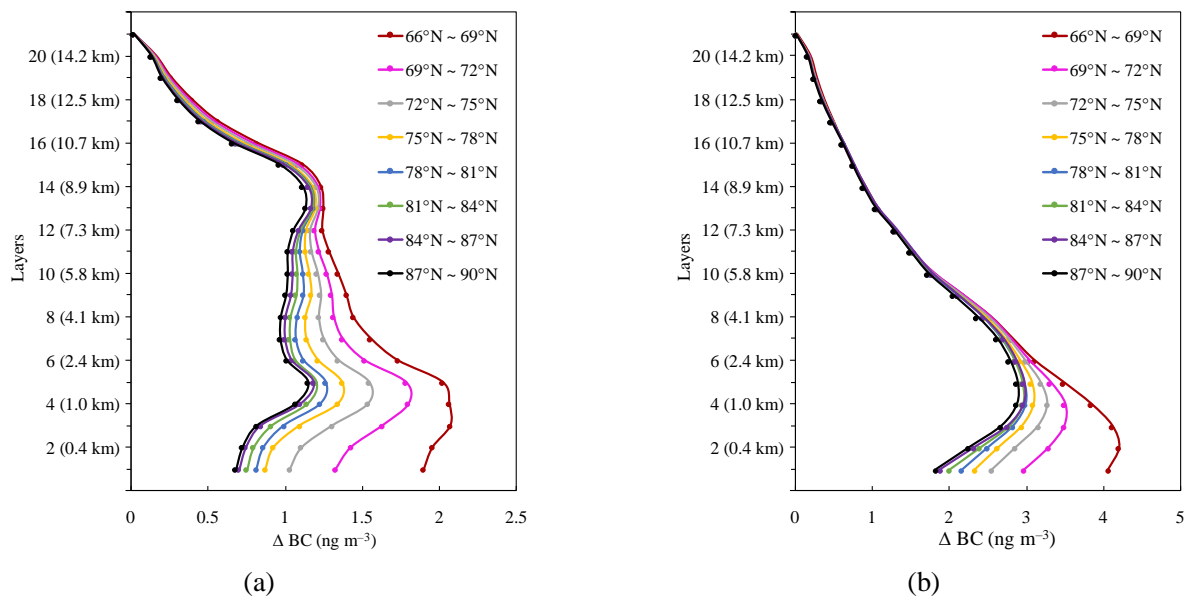
Figure 7. Contributions of 20% emission reductions from all six source regions to the vertical BC concentrations of the Arctic in different latitude bands varies with vertical layers in **(a)** summer and **(b)** winter in 2010.

As same as the whole Arctic region (Section 3.3.1 & 3.3.2), the contributions of 20% emission reductions to BC concentrations in eight latitude bands were higher in winter than in summer, whether near surface or in vertical. The contribution of 20% emission reductions from all six source regions to BC concentrations in eight latitude bands of the Arctic near surface was 0.7–1.9 ng m^{-3} in

496 summer and 1.8–4.1 ng m^{-3} in winter, respectively (Figure 6). The high BC peak at around 0.6–1.6

497 km a.s.l. (3rd – 5th layers) was 1.1–2.1 ng m^{-3} in summer, and 2.9–4.2 ng m^{-3} in winter (Figure 7).

498 **3.4 Benefit of BC emission reductions on the decrease of Arctic temperature**

499 The impact of BC emission reductions on decreasing the Arctic (60–90°N) surface temperature was

500 assessed by using ARTP (See methods in Section 2.2). Aerosol effects, BC deposition on snow, and

501 BC semi-direct were considered in the calculation of ARTP (Aamaas et al., 2017). As shown in

502 Figure 8, the response of Arctic surface temperature to emission reductions was the most significant

503 at the time scale of 10 years and then gradually decreased with the passage of time. For each source

504 region, the Arctic temperature response was significantly higher in winter than in summer as ARTP

505 was seasonal dependent with higher values in the colder seasons. Obviously, the Arctic surface

506 temperature benefited the most from BC emission reductions from EAS with more than 300 and 660

507 μK decreases in summer and winter after 10 years, respectively. The influences of EUR and NAM

508 emission reductions on the temperature decrease were similar in summer, reaching about 3–90 μK

509 after 10, 20, 50, and 100 years. However, in winter, the influence of emission reductions from NAM

510 on temperature decrease (8–200 μK) was weaker than that from EUR (14–370 μK). This was mainly

511 due to the difference of ARTPs between EUR and NAM was not obvious compared with the

512 difference of emission reductions from NAM and EUR in summer and winter. The responses of the

513 temperature decrease to emission reductions from RBU were 9–20 μK in summer and 4–100 μK in

514 winter after 10-100years, respectively, which were smaller than that from EUR and NAM. This can

515 be explained by the low BC emission reductions from RBU (Table 1). The response of the

516 temperature decrease to emission reductions from SAS in winter (10–320 μK) was similar to that

517 from EUR, while this response in summer (8–230 μK) was more than twice that of EUR. Although

518 the ARTP of EUR was higher than that of SAS, the BC emission reductions from SAS were much

519 higher than that from EUR and the difference between emission reductions from the two regions was

520 more obvious in summer (Table 1). In spite of the higher Arctic temperature response to EAS than

521 SAS in the target year of this study, a number of studies have shown that BC emissions in South Asia

522 were increasing in recent years (Sahu et al., 2008; Paliwal et al., 2016; Sharma et al., 2019) while the

523 emissions of East Asia were exhibiting a downward trend especially from China (Chen et. al., 2016),

524 thus it should be given more attention to the impact assessment of South Asia on the Arctic in the

future. The minimum temperature response was found from MDE due to the least emission reductions and small ARTP.

(a)

(b)
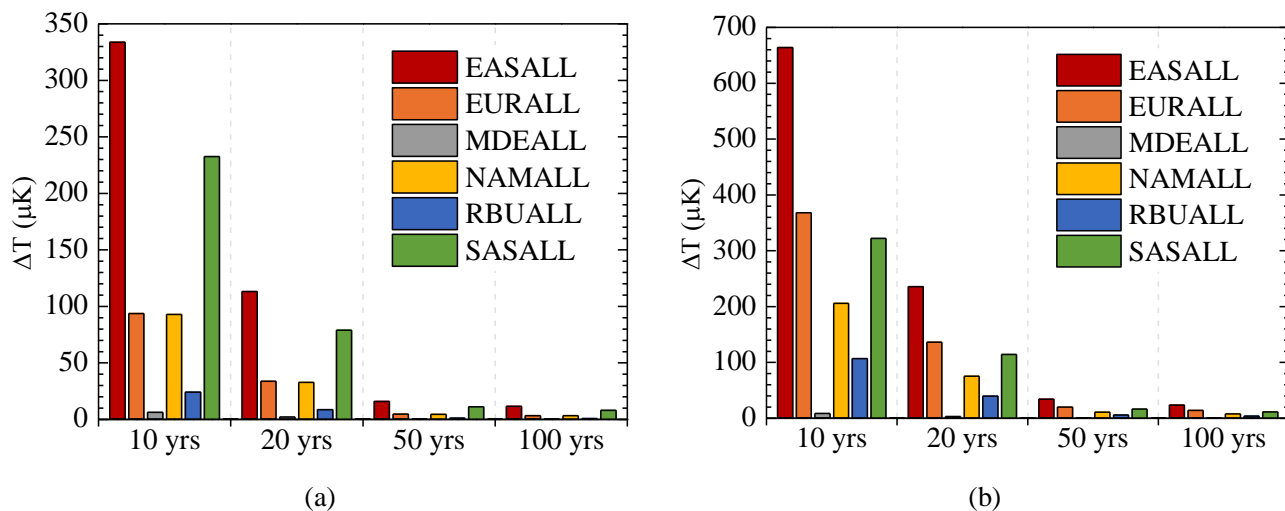
Figure 8. Arctic surface temperature response to 20% regional BC emission reductions in **(a)** summer and **(b)** winter after 10, 20, 50, and 100 years.

In addition, the impacts of BC emission reductions from six source regions on the Arctic and global surface temperature were compared in this study (Figure 9). Due to the BC emission reductions from the six source regions, the surface temperature in the Arctic decreased 27–780 µK in summer and 61–1675 µK in winter after 10, 20, 50, and 100 years, which were higher than that of the global with the values of 10–290 µK in summer and 16–470 µK in winter. It can be seen that the difference of the temperature response between the Arctic and the globe was more obvious in winter. Overall, the response of the Arctic surface temperature was more sensitive to emissions perturbation than that of the globe surface temperature.

(a)

(b)
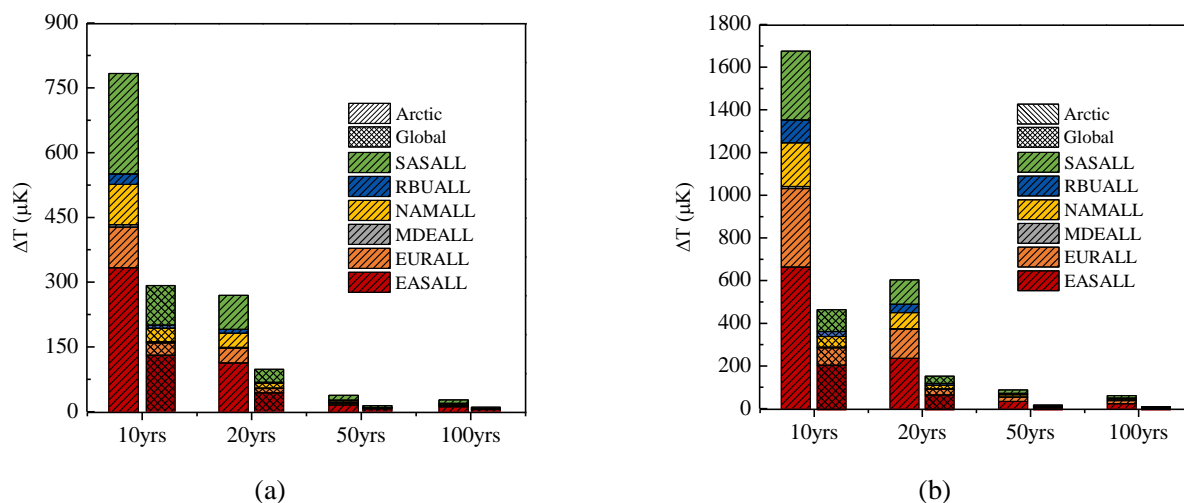
Figure 9. Global and Arctic surface temperature responses to 20% regional BC emission reductions in **(a)** summer and **(b)** winter after 10, 20, 50, and 100 years.

It should be noted the estimation of temperature response was subject to large uncertainties for the following reasons. On the one hand, even though the HTAP2 emissions database were all constructed by bottom-up methods, the different inventories and spatiotemporal distributions were constructed with sub-regional (country, state, county or province level) activity data and emission factors, which lead to inconsistencies at the borders between two adjacent inventories. The version 5 of Evaluating the Climate and Air Quality Impacts of Short-Lived Pollutants (ECLIPSEv5, http://eclipse.nilu.no) estimated a 2010 emission inventory, that serves also as a reference point for all projections (Janssens-Maenhout et al., 2015). At the global level, a relatively good agreement was found with small relative emission differences compared with the ECLIPSEv5 emission inventory for the aggregated sectors in 2010. However, larger differences of 29% between HTAP2 and ECLIPSEv5 emissions was present for BC since ECLIPSEv5 relied on provincial statistics for China which resulted from higher coal consumption than reported national statistics. Hoesly et al. (2018) provided a sectoral and gridded historical (1750–2014) anthropogenic emission inventory for use in the Coupled Model Intercomparison Project phase 6 (CMIP6). The amount of global BC anthropogenic emissions was 7.7 Tg/year in 2010 from the CMIP6 emissions, which was larger than that from HTAP2 emissions (5.5 Tg/year). This was mainly due to the energy, transportation, and international shipping sectors of CMIP6 were higher than those of HTAP2.

On the other hand, the time evolution of R_T, a parameter in the calculation of ARTP was also one factor causing the uncertainty of temperature response calculation. This impulse response function was only based on one coupled atmosphere-ocean climate model GISS-ER in this study, while Olivié and Peters (2013) have found a spread in the GTP (20) value of BC of about −60 to +80% due to variability of R_T among various models. However, the uncertainty in R_T was less relevant for the regional patterns. Forcing-response coefficients didn't exist on a seasonal basis since emissions occurring during Northern Hemisphere summer and winter season were differentiated (Aamaas et al, 2017). Hence, the seasonal differences presented here in the ARTP values were not due to potential differences in the response sensitivities, but due to differences in the RF. The temperature response will vary by species and location, such as between land surface and ocean surface. These differences are not accounted for in this study, but the increased efficacy in the RCS matrix towards the NH can

569 be partly attributed to a larger land area fraction in the NH (Shindell et al., 2015). Besides, recent
570 studies have found that the positive radiation budget of BC being largely compensated for by rapid
571 atmospheric adjustment, this means that the responses of surface temperatures to BC tends to be
572 weaker than expected (Stjern et al., 2017; Takemura and Suzuki, 2019).

573   Although the HTAP2 emissions database contain uncertainties and ARTP calculations are
574 simplifications, these emission metrics are useful, simple, and quick approximations for calculating
575 the temperature response in the different latitude bands for emissions of BC.

4. Conclusions

577 The CAMchem, CHASER_re1, GEOS-Chem, GOCART, and Oslo CTM3 in HTAP2 experiment
578 were used in this study to estimate the responses of Arctic BC to multi-region emission reductions in
579 2010. Six regions (e.g., EAS, EUR, MDE, RBU, NAM, and SAS) were selected as the source
580 regions and the Arctic was the receptor region. HTAP2 set up the base scenario with all BC
581 emissions, and also simulated BC concentrations with 20% reduction of anthropogenic emissions.
582 The AGPT was further used to calculate the benefit of BC emission reductions on the decrease of
583 Arctic temperature.

584   The statistical results of 20% BC emission reductions showed that emission reductions in EAS
585 were the largest with the values of 355.6 Gg yr^{-1}, followed by SAS (232.5 Gg yr^{-1}), EUR (65.3 Gg
586 yr^{-1}), NAM (62.2 Gg yr^{-1}), RBU (18.6 Gg yr^{-1}), and MDE (5.3 Gg yr^{-1}). The BC emission
587 reductions in the EAS, EUR, and RBU were higher from November to March.

588   The temporal variations of simulations from different models were relatively consistent as the
589 correlations of the simulated BC concentrations among different models ranged from 0.33 to 0.98.
590 However, the simulated BC concentrations didn't agree so well with observations at monitoring sites
591 except Zeppelin. In order to reduce the difference of simulation performance of each model in
592 different areas of the Arctic, the model ensemble mean was used for analysis.

593   The contribution of 20% BC emission reductions from EAS, EUR, MDE, NAM, RBU, and SAS
594 to the Arctic near-surface BC concentrations reached 0.70, 0.54, 0.01, 0.20, 0.29, and 0.09 ng m^{-3},
595 respectively. Correspondingly, the reduced column BC loadings from the six regions above over the
596 Arctic was 8521.7, 2789.1, 28.8, 1762.1, 998.6, and 3640.2 ng m^{-2}, respectively.

597   The response of Arctic near-surface BC concentrations to 20% emission reductions from EAS and

598   EUR was larger than other four source regions, with the monthly value of 0.2–1.5 ng m^{-3} and 0.2–1.0

599   ng m^{-3}, accounting for 16.8%–49.0% and 20.1%–49.0% of the total contributions from all six

600   regions, respectively. The BC profiles displayed a bimodal pattern in summer with peaks at around

601   1.0–1.6 km a.s.l. (4th and 5th layers) and 8.0–8.9 km a.s.l. (13th and 14th layers). While the BC profiles

602   showed a unimodal pattern with peaks around 0.6–1.6 km a.s.l. (3rd – 5th layers) in winter.

603   The response of Arctic BC to emission reductions from source regions in winter was higher than

604   that in summer. The contributions of 20% emission reductions to the Arctic BC concentrations near

605   surface were the highest between 66–69°N both in summer (1.9 ng m^{-3}) and winter (4.1 ng m^{-3}), and

606   became weaker with the increase of the latitude.

607   The response of Arctic temperature to BC emission reductions was the most significant at the time

608   scale of 10 years and then gradually decreased with the passage of time. The Arctic had benefited the

609   most from emission reduction in EAS with more than 300 and 660 μK decreases in summer and

610   winter after 10 years, respectively. The Arctic temperature response was more sensitive to the whole

611   globe in regard of the same emissions perturbation. The estimation of temperature response was

612   subject to large uncertainties due to the uncertainties in the calculation of ARTP and emissions of BC

613   in source regions.

614   Overall, this study provided insights on the source regions and seasonal contributions of Arctic BC

615   from the most recent international ensemble modeling efforts. The discrepancy between model

616   results and observations and the spread among different HTAP models may be attributed to various

617   factors such as emissions in the remote Arctic, physical parameterizations, and convection and

618   deposition processes. This would subsequently result in large uncertainties of the climatic effects of

619   air pollutants. More observation sites on the typical transport pathways from sources regions to the

620   Arctic should be planned to improve the model capability of simulating the transport behavior of

621   black carbon.

622 **Data availability**

623   All data used in this paper can be obtained through the AeroCom servers and web interfaces,

624   accessible at http://aerocom.met.no.

625

Author contributions

627 KH and JSF designed this study. ML, KS, DH, TK, MC, and ST performed modeling. NZ analyzed

628 data and wrote the paper. All have commented on and reviewed the paper.

629

Competing interests.

631 The authors declare that they have no conflict of interest.

632

Acknowledgements

634 We sincerely thank for the HTAPv2 international initiative. This work was partially supported by

635 the National Natural Science Foundation of Shanghai (18230722600), the National Key R&D

636 Program of China (2018YFC0213105), and the National Natural Science Foundation of China

637 (91644105).

638

References

Aamaas, B., Berntsen, T. K., Fuglestvedt, J. S., Shine, K. P., and Bellouin, N.: Regional emission metrics for short–lived climate forcers from multiple models, Atmos. Chem. Phys., 16, 7451– 7468, https://doi.org/10.5194/acp–16–7451–2016, 2016.

Aamaas, B., Berntsen, T. K., Fuglestvedt, J. S., Shine, K. P., and Collins, W. J.: Regional temperature change potentials for short-lived climate forcers based on radiative forcing from multiple models, Atmos. Chem. Phys., 17, 10795-10809, 10.5194/acp-17-10795-2017, 2017.

AMAP: Black carbon and ozone as Arctic climate forcers. Arctic Monitoring and Assessment Programme (AMAP), Oslo, Norway. vii + 116 pp, 2015.

AMAP: Snow, Water, Ice and Permafrost in the Arctic (SWIPA) 2017. Arctic Monitoring and Assessment Programme (AMAP), Oslo, Norway. xiv + 269 pp. ISBN 978–82–7971–101–8, 2017.

AMAP: The Impact of Black Carbon on Arctic Climate. By: Quinn, P. K., Stohl, A., Arneth, A., Berntsen, T., Burkhart, J. F., Christensen, J., Flanner, M., Kupiainen, K., Lihavainen, H., Shepherd, M., Shevchenko, V., Skov, H., and Vestreng., V., Arctic Monitoring and Assessment Programme (AMAP), Oslo. 72 pp, 2011.

AMAP: The Impact of Short–Lived Pollutants on Arctic Climate. By: Quinn, P. K., Bates, T. S., Baum, E., Bond, T., Burkhart, J. F., Fiore, A. M., Flanner, M. G., Garrett, T., Koch, D., Mcconnell, J. R., Shindell, D., and Stohl, A., Arctic Monitoring and Assessment Programme (AMAP), Oslo, Norway, 2008.

Barrie, L. A.: Arctic air pollution: an overview of current knowl- edge, Atmos. Environ., 20, 643–663, 1986.

Bond, T. C., Doherty, S. J., Fahey, D. W., Forster, P. M., Berntsen, T., DeAngelo, B. J., Flanner, M. G., Ghan, S., Kärcher, B., Koch, D., Kinne, S., Kondo, Y., Quinn, P. K., Sarofim, M. C., Schultz, M. G., Schulz, M., Venkataraman, C., Zhang, H., Zhang, S., Bellouin, N., Guttikunda, S. K., Hopke, P. K., Jacobson, M. Z., Kaiser, J. W., Klimont, Z., Lohmann, U., Schwarz, J. P., Shindell, D., Storelvmo, T., Warren, S. G., and Zender, C. S.: Bounding the role of black carbon in the climate system: A scientific assessment, J. Geophys. Res.–Atmos., 118, 5380–5552, https://doi.org/10.1002/jgrd.50171, 2013.

Bozem, H., Hoor, P., Kunkel, D., Köllner, F., Schneider, J., Herber, A., Schulz, H., Leaitch, W. R., Aliabadi, A. A., Willis, M. D., Burkart, J., and Abbatt, J. P. D.: Characterization of transport regimes and the polar dome during Arctic spring and summer using in situ aircraft measurements, Atmos. Chem. Phys., 19, 15049-15071, 10.5194/acp-19-15049-2019, 2019.

Bradley, R. S., Keimig, F. T., and Diaz, H. F.: Climatology of surface-based inversions in the North American Arctic, J. Geophys. Res., 97, 15 699, https://doi.org/10.1029/92JD01451, 1992.

Chen, D. S., Zhao, Y. H., Nelson, P., Li, Y., Wang, X. T., Zhou, Y., Lang, J. L., and Guo, X. R.: Estimating ship emissions based on AIS data for port of Tianjin, China. Atmos. Environ. 145: 10–18. http://dx.doi.org/10.1016/j.atmosenv.2016.

Cheng, G.: Analysis of observational data of atmospheric boundary layer characteristics in the Arctic (in Chinese), Nanjing University of information engineering. 2011.

Chin, M., Rood, R. B., Lin, S.–J., Müller, J.–F., and Thompson, A. M.: Atmospheric sulfur cycle simulated in the global model GOCART: Model description and global properties, J. Geophys. Res.–Atmos., 105, 24671–24687, doi:10.1029/2000JD900384, 2000.

Clarke, A. D. and Noone, K. J.: Soot in the Arctic snowpack: a cause for perturbations in radiative transfer, Atmos. Environ., 19, 2045–2053, https://doi.org/10.1016/0004-6981(85)90113-1, 1985.

Collins, W. J., Fry, M. M., Yu, H., Fuglestvedt, J. S., Shindell, D. T., and West, J. J.: Global and regional

temperature-change potentials for near-term climate forcers, Atmos. Chem. Phys., 13, 2471-2485, 10.5194/acp-13-2471-2013, 2013.

Eckhardt, S., Stohl, A., Beirle, S., Spichtinger, N., James, P., Forster, C., Junker, C., Wagner, T., Platt, U., and Jennings, S. G.: The North Atlantic Oscillation controls air pollution transport to the Arctic, Atmos. Chem. Phys., 3, 1769–1778, https://doi.org/10.5194/acp–3–1769–2003, 2003.

Flanner, M. G.: Arctic climate sensitivity to local black carbon, J. Geophys. Res.-Atmos., 118, 1840–1851, https://doi.org/10.1002/jgrd.50176, 2013.

Fuglestvedt, J. S., Shine, K. P., Berntsen, T., Cook, J., Lee, D. S., Stenke, A., Skeie, R. B., Velders, G. J. M., and Waitz, I. A.: Transport impacts on atmosphere and climate: metrics, Atmos. Environ., 44, 4648–4677, https://doi:10.1016/j.atmosenv.2009.04.044, 2010.

Galmarini, S., Koffi, B., Solazzo, E., Keating, T., Hogrefe, C., Schulz, M., Benedictow, A., Griesfeller, J. J., Janssens-Maenhout, G., Carmichael, G., Fu, J., and Dentener, F.: Technical note: Coordination and harmonization of the multi-scale, multi-model activities HTAP2, AQMEII3, and MICS-Asia3: simulations, emission inventories, boundary conditions, and model output formats, Atmos. Chem. Phys., 17, 1543–1555, 2017.

Garrett, T. J. and Zhao, C.: Increased Arctic cloud longwave emissivity associated with pollution from mid-latitudes, Nature, 440, 787–789, 2006.

Hansen, J. and Nazarenko, L.: Soot climate forcing via snow and ice albedos, P. Natl Acad. Sci. USA, 101, 423–428, https://doi.org/10.1073/pnas.2237157100, 2004.

Henze, D. K., Hakami, A., and Seinfeld, J. H.: Development of the adjoint of GEOS–Chem, Atmos. Chem. Phys., 7, 2413–2433, doi:10.5194/acp–7–2413–2007, 2007.

Hoesly R. M., Smith S. J., Feng L. Y., Klimont Z., Janssens-Maenhout G., Pitkanen T., Seibert J. J., Vu L., Andres R. J., Bolt R. M., Bond T. C., Dawidowski L., Kholod N., Kurokawa J., Li M., Liu L., Lu Z. F., Moura M. C. P., O'Rourke P. R., Zhang Q.: Historical (1750–2014) anthropogenic emissions of reactive gases and aerosols from the Community Emissions Data System (CEDS), Geosci. Model Dev., 11, 369–408, 10.5194/gmd-11-369-2018, 2018.

Hogrefe, C., Liu, P., Pouliot, G., Mathur, R., Roselle, S., Flemming, J., Lin, M., and Park, R. J.: Impacts of different characterizations of large-scale background on simulated regional-scale ozone over the continental United States, Atmos. Chem. Phys., 18, 3839–3864, 2018.

Huang, K., Fu, J. S., Hodson, E. L., Dong, X., Cresko, J., Prikhodko, V. Y., Storey, J. M., and Cheng, M.-D.: Identification of missing anthropogenic emission sources in Russia: Implication for modeling Arctic haze, Aerosol Air Qual. Res., 14, 1799–1811, 2014.

Huang, K., Fu, J. S., Prikhodko, V. Y., Storey, J. M., Ro- manov, A., Hodson, E. L., Cresko, J., Morozova, I., Ig- natieva, Y., and Cabaniss, J.: Russian anthropogenic black carbon: Emission reconstruction and Arctic black carbon simulation, J. Geophys. Res.-Atmos., 120, 11306–11333, https://doi.org/10.1002/2015JD023358, 2015.

IPCC: Climate Change: The Intergovernmental Panel on Climate Change Scientific Assessment. The Intergovernmental Panel on Climate Change (IPCC), Cambridge University Press, Cambridge, UK, 1990.

IPCC: Climate Change 2001: The Scientific Basis. Intergovernmental Panel on Climate Change. The Intergovernmental Panel on Climate Change (IPCC), Cambridge University Press, Cambridge, UK, 2001.

Janssens-Maenhout, G., Crippa, M., Guizzardi, D., Dentener, F., Muntean, M., Pouliot, G., Keating, T., Zhang, Q., Kurokawa, J., Wankmüller, R., Denier van der Gon, H., Kuenen, J. J. P., Klimont, Z., Frost, G., Darras, S., Koffi, B., and Li, M.: HTAP_v2.2: a mosaic of regional and global emission grid maps for 2008 and 2010 to study hemispheric transport of air pollution, Atmos. Chem. Phys., 15, 11411-11432, 10.5194/acp-15-11411-2015, 2015.

Jonson, J. E., Schulz, M., Emmons, L., Flemming, J., Henze, D., Sudo, K., Tronstad Lund, M., Lin, M., Benedictow,

725 A., Koffi, B., Dentener, F., Keating, T., Kivi, R., and Davila, Y.: The effects of intercontinental emission
726   sources on European air pollution levels, Atmos. Chem. Phys., 18, 13655–13672, 2018.

727 Koch, D. and Hansen, J.: Distant origins of Arctic black carbon: A Goddard Institute for Space Studies ModelE
728   experiment, J. Geophys. Res.–Atmos., 110, D04204, https://doi.org/10.1029/2004JD005296, 2005.

729 Lamarque, J. F., Emmons, L. K., Hess, P. G., Kinnison, D. E., Tilmes, S., Vitt, F., Heald, C. L., Holland, E. A.,
730   Lauritzen, P. H., Neu, J., Orlando, J. J., Rasch, P. J., and Tyndall, G. K.: CAM-chem: description and
731   evaluation of interactive atmospheric chemistry in the Community Earth System Model, Geosci. Model Dev.,
732   5, 369-411, 10.5194/gmd-5-369-2012, 2012.

733 Law, K. S. and Stohl, A.: Arctic air pollution: origins and impacts, Science, 315, 1537–1540,
734   https://doi.org/10.1126/science.1137695, 2007.

735 Liang, C.-K., West, J. J., Silva, R. A., Bian, H., Chin, M., Davila, Y., Dentener, F. J., Emmons, L., Flemming, J.,
736   Folberth, G., Henze, D., Im, U., Jonson, J. E., Keating, T. J., Kucsera, T., Lenzen, A., Lin, M., Lund, M. T., Pan,
737   X., Park, R. J., Pierce, R. B., Sekiya, T., Sudo, K., and Takemura, T.: HTAP2 multi-model estimates of
738   premature human mortality due to intercontinental transport of air pollution and emission sectors, Atmos.
739   Chem. Phys., 18, 10497–10520, 2018.

740 Lund, M. T., Berntsen, T. K., Heyes, C., Klimont, Z., and Samset, B. H.: Global and regional climate impacts of
741   black carbon and co-emitted species from the on-road diesel sector, Atmos. Envi- ron., 98, 50–58,
742   https://doi.org/10.1016/j.atmosenv.2014.08.033, 2014.

743 Lund, M. T., Aamaas, B., Berntsen, T., Bock, L., Burkhardt, U., Fuglestvedt, J. S., and Shine, K. P.: Emission
744   metrics for quantifying regional climate impacts of aviation, Earth Syst. Dynam., 8, 547–563,
745   https://doi.org/10.5194/esd-8-547-2017, 2017.

746 Lund, M. T., Myhre, G., Haslerud, A. S., Skeie, R. B., Griesfeller, J., Platt, S. M., Kumar, R., Myhre, C. L., and
747   Schulz, M.: Concentrations and radiative forcing of anthropogenic aerosols from 1750 to 2014 simulated with
748   the Oslo CTM3 and CEDS emission inventory, Geosci. Model Dev., 11, 4909–4931,
749   https://doi.org/10.5194/gmd-11-4909-2018, 2018.

750 Marelle, L., Thomas, J. L., Raut, J.-C., Law, K. S., Jalkanen, J.- P., Johansson, L., Roiger, A., Schlager, H., Kim, J.,
751   Reiter, A., and Weinzierl, B.: Air quality and radiative impacts of Arctic shipping emissions in the summertime
752   in northern Norway: from the local to the regional scale, Atmos. Chem. Phys., 16, 2359– 2379,
753   https://doi.org/10.5194/acp-16-2359-2016, 2016.

754 Miao, Y. C., Guo, J. P., Liu, S. H., Liu, H., Zhang, G., Yan, Y., He, J.: Relay transport of aerosols to
755   Beijing–Tianjin–Hebei region by multiscale atmospheric circulations, Atmos. Environ., 165, 35–45,
756   https://doi.org/10.1016/j.atmosenv.2017.06.032, 2017.

757 Myhre, G., Shindell, D., Breon, F.–M., Collins, W., Fuglestvedt, J., Huang, J., Koch, D., Lamarque, J.–F., Lee, D.,
758   Mendoza, B., Nakajima, T., Robock, A., Stephens, G., Takemura, T., and Zhang, H.: Anthropogenic and
759   Natural Radiative Forcing, in: Climate Change 2013: The Physical Science Basis. Contribution of Working
760   Group I to the Fifth Assessment Report of the Inter– governmental Panel on Climate Change, edited by:
761   Stocker, T. F., Qin, D., Plattner, G.–K., Tignor, M., Allen, S. K., Boschung, J., Nauels, A., Xia, Y., Bex, V., and
762   Midgley, P. M., Cambridge Uni– versity Press, Cambridge, UK and New York, NY, USA, 2013.

763 Olivié, D. J. L. and Peters, G. P.: Variation in emission metrics due to variation in CO2 and temperature impulse
764   response functions, Earth Syst. Dynam., 4, 267–286, https://doi.org/10.5194/esd-4- 267-2013, 2013.

765 Paliwal, U., Sharma, M., and Burkhart, J. F.: Monthly and spatially resolved black carbon emission inventory of
766   India: uncertainty analysis, Atmos. Chem. Phys., 16, 12457-12476, 10.5194/acp-16-12457-2016, 2016.

767 Sahu, S. K., Beig, G., and Sharma, C.: Decadal growth of black carbon emissions in India, Geophysical Research
768   Letters, 35, 10.1029/2007gl032333, 2008.

769 Samset, B. H., Myhre, G., Schulz, M., Balkanski, Y., Bauer, S., Berntsen, T. K., Bian, H., Bellouin, N., Diehl, T.,

Easter, R. C., Ghan, S. J., Iversen, T., Kinne, S., Kirkevåg, A., Lamarque, J. F., Lin, G., Liu, X., Penner, J. E., Seland, Ø., Skeie, R. B., Stier, P., Takemura, T., Tsigaridis, K., and Zhang, K.: Black carbon vertical profiles strongly affect its radiative forcing uncertainty, Atmos. Chem. Phys., 13, 2423-2434, 10.5194/acp-13-2423-2013, 2013.

Sand, M., Berntsen, T. K., von Salzen, K., Flanner, M. G., Langner, J., and Victor, D. G.: Response of Arctic temperature to changes in emissions of short–lived climate forcers, Nature Clim. Change, 6, 286–289, 10.1038/nclimate2880, 2016.

Sekiya, T., Miyazaki, K., Ogochi, K., Sudo, K., and Takigawa, M.: Global high-resolution simulations of tropospheric nitrogen dioxide using CHASER V4.0, Geosci. Model Dev., 11, 959-988, 10.5194/gmd-11-959-2018, 2018.

Sharma, S., Ishizawa, M., Chan, D., Lavoué, D., Andrews, E., Eleftheriadis, K., and Maksyutov, S.: 16-year simulation of Arctic black carbon: Transport, source contribution, and sensitivity analysis on deposition, Journal of Geophysical Research: Atmospheres, 118, 943-964, 10.1029/2012jd017774, 2013.

Sharma, G., Sinha, B., Pallavi, Hakkim, H., Chandra, B. P., Kumar, A., and Sinha, V.: Gridded Emissions of CO, NO_x, SO_2, CO_2, NH_3, HCl, CH_4, $PM_{2.5}$, PM_{10}, BC, and NMVOC from Open Municipal Waste Burning in India, Environ Sci Technol, 53, 4765-4774, 10.1021/acs.est.8b07076, 2019.

Shine, K. P., Fuglestvedt, J. S., Hailemariam, K., and Stuber, N.: Alternatives to the Global Warming Potential for Comparing Climate Impacts of Emissions of Greenhouse Gases, Climatic Change, 68, 281–302, 10.1007/s10584–005–1146–9, 2005

Shindell, D. and Faluvegi, G.: Climate response to regional radiative forcing during the 20th century, Nat. Geosci., 2, 294–300, 2009.

Shindell, D. and Faluvegi, G.: The net climate impact of coal–fired power plant emissions, Atmos. Chem. Phys., 10, 3247–3260, https://doi.org/10.5194/acp–10–3247–2010, 2010.

Shindell D., Kuylenstierna J.C.I., Vignati E., van Dingenen R., Amann M., Klimont Z., Anenberg S.C., Muller N., JanssensMaenhaut G., Raes F., Schwartz J., Faluvegi G., Pozzoli L., Kupiainen K., Höglund–Isaksson L., Emberson L., Streets D., Ramanathan V., Hicks K., Kim Oanh N.T., Milly G., Williams M., Demkine W., Fowler D.: Simultaneously Mitigating Near–Term Climate Change and Improving Human Health and Food Security. Science, Vol. 335, 183–189, 2012.

Shindell, D. T., Chin, M., Dentener, F., Doherty, R. M., Faluvegi, G., Fiore, A. M., Hess, P., Koch, D. M., MacKenzie, I. A., Sanderson, M. G., Schultz, M. G., Schulz, M., Stevenson, D. S., Teich, H., Textor, C., Wild, O., Bergmann, D. J., Bey, I., Bian, H., Cuvelier, C., Duncan, B. N., Folberth, G., Horowitz, L. W., Jonson, J., Kaminski, J. W., Marmer, E., Park, R., Pringle, K. J., Schroeder, S., Szopa, S., Takemura, T., Zeng, G., Keating, T. J., Zuber, A.: A multi–model assessment of pollution transport to the Arctic, Atmos. Chem. Phys. Discuss., 2008.

Shindell, D. T., Faluvegi, G., Rotstayn, L., and Milly, G.: Spatial patterns of radiative forcing and surface temperature response, J. Geophys. Res.-Atmos., 120, 5385–5403, https://doi.org/10.1002/2014JD022752, 2015.

Shindell, D. T., Lamarque, J.–F., Schulz, M., Flanner, M., Jiao, C., Chin, M., Young, P. J., Lee, Y. H., Rotstayn, L., Mahowald, N., Milly, G., Faluvegi, G., Balkanski, Y., Collins, W. J., Conley, A. J., Dalsoren, S., Easter, R., Ghan, S., Horowitz, L., Liu, X., Myhre, G., Nagashima, T., Naik, V., Rumbold, S. T., Skeie, R., Sudo, K., Szopa, S., Takemura, T., Voulgarakis, A., Yoon, J.–H., and Lo, F.: Radiative forcing in the ACCMIP historical and future climate simulations, Atmos. Chem. Phys., 13, 2939–2974, 2013.

Shindell, D. T., Voulgarakis, A., Faluvegi, G., and Milly, G.: Precipitation response to regional radiative forcing, Atmos. Chem. Phys., 12, 6969–6982, doi:10.5194/acp–12–6969–2012, 2012.

Smith, S.J. and Mizrahi, A.: Near–term climate mitigation by short–lived forcers. PNAS 14202–14206, doi:

815   10.1073/pnas.1308470110, 2013.

816 Sobhani, N., Kulkarni, S., Carmichael, G. R.: Source sector and region contributions to black carbon and PM$_{2.5}$ in
817   the Arctic. Atmos. Chem. Phys., 18, 18123–18148, 2018.

818 Stjern, C. W., Samset, B. H., Myhre, G., Bian, H., Chin, M., Davila, Y., Dentener, F., Emmons, L., Flemming, J.,
819   Haslerud, A. S., Henze, D., Jonson, J. E., Kucsera, T., Lund, M. T., Schulz, M., Sudo, K., Takemura, T., and
820   Tilmes, S.: Global and regional radiative forcing from 20 % reductions in BC, OC and SO4 – an HTAP2
821   multi-model study, Atmos. Chem. Phys., 16, 13579–13599, https://doi.org/10.5194/acp-16-13579-13599,
822   2016.

823 Stjern, C. W. et al. Rapid adjustments cause weak surface temperature response to increased black carbon
824   concentrations. Geophys. Res. 122, 11462–11481, 2017.

825 Stohl, A.: Characteristics of atmospheric transport into the Arctic troposphere, J. Geophys. Res., 111, D11306,
826   https://doi.org/10.1029/2005JD006888, 2006.

827 Stohl A., Aamaas B., Amann M., Baker L. H., Bellouin N., Berntsen T. K., Boucher O., Cherian R., Collins W.,
828   Daskalakis N., Dusinska M., Eckhardt S., Fuglestvedt J. S., Harju M., Heyes C., Hodnebrog Ø., Hao J., Im U.,
829   Kanakidou M., Klimont Z., Kupiainen K., Law K. S., Lund M. T., Maas R., MacIntosh C. R., Myhre G.,
830   Myriokefalitakis S., Olivié D., Quaas J., Quennehen B., Raut J.–C., Rumbold S. T., Samset B. H., Schulz M.,
831   Seland Ø., Shine K. P., Skeie R. B., Wang S., Yttri K. E., and Zhu T.: Evaluating the climate and air quality
832   impacts of short–lived pollutants. Atmos. Chem. Phys., 15, 10529 – 10566, 2015.

833 Stohl, A., Eckhardt, S., Forster, C., James, P., and Spichtinger, N.: On the pathways and timescales of
834   intercontinental air pollution transport, J. Geophys. Res.–Atmos., 107, ACH 6–1–ACH 6–17,
835   https://doi.org/10.1029/2001JD001396, 2002.

836 Stohl, A., Klimont, Z., Eckhardt, S., Kupiainen, K., Shevchenko, V. P., Kopeikin, V. M., and Novigatsky, A. N.:
837   Black carbon in the Arctic: the underestimated role of gas flaring and residential combustion emissions, Atmos.
838   Chem. Phys., 13, 8833–8855, https://doi.org/ 10.5194/acp-13-8833-2013, 2013

839 Sudo, K., Sekiya, T., Nagashima, T.: CHASER/MIROC-ESM in HTAP2 status reports, HTAP2 Global and
840   Regional Model Evaluation Workshop, Nagoya University, JAMSTEC, NIES, 2015.

841 Sudo, K., Takahashi, M., Kurokawa, J.–I., and Akimoto, H.: CHASER: A global chemical model of the troposphere
842   1. Model description, J. Geophys. Res.–Atmos., 107, ACH 7–1–ACH 7–20, doi:10.1029/2001JD001113,
843   2002.

844 Søvde, O. A., Prather, M. J., Isaksen, I. S. A., Berntsen, T. K., Stordal, F., Zhu, X., Holmes, C. D., and Hsu, J.: The
845   chemical transport model Oslo CTM3, Geosci. Model Dev., 5, 1441–1469, doi:10.5194/gmd–5–1441–2012,
846   2012.

847 Takemura, T., and Suzuki, K.: Weak global warming mitigation by reducing black carbon emissions, Scientific
848   Reports, 9, 10.1038/s41598-019-41181-6, 2019.

849 Tan, J., Fu, J. S., Dentener, F., Sun, J., Emmons, L., Tilmes, S., Sudo, K., Flemming, J., Jonson, J. E., Gravel, S.,
850   Bian, H., Davila, Y., Henze, D. K., Lund, M. T., Kucsera, T., Takemura, T., and Keating, T.: Multi-model study
851   of HTAP II on sulfur and nitrogen deposition, Atmos. Chem. Phys., 18, 6847–6866, 2018a.

852 Tan, J., Fu, J. S., Dentener, F., Sun, J., Emmons, L., Tilmes, S., Flemming, J., Takemura, T., Bian, H., Zhu, Q., Yang,
853   C.-E., and Keating, T.: Source contributions to sulfur and nitrogen deposition – an HTAP II multi-model study
854 on hemispheric transport, Atmos. Chem. Phys., 18, 12223–12240, 2018b.

855 Teng, H., Washington, W. M., Branstator, G., Meehl, G. A., and Lamarque, J.–F.: Potential impacts of Asian carbon
856   aerosols on future US warming, Geophys. Res. Lett., 39, L11703, doi:10.1029/2012GL051723, 2012.

857 Tilmes, S., Lamarque, J.–F., Emmons, L. K., Kinnison, D. E., Marsh, D., Garcia, R. R., Smith, A. K., Neely, R. R.,
858   Conley, A., Vitt, F., Val Martin, M., Tanimoto, H., Simpson, I., Blake, D. R., and Blake, N.: Representation of
859   the Community Earth System Model (CESM1) CAM4–chem within the Chemistry– Climate Model Initiative

860   (CCMI), Geosci. Model Dev., 9, 1853– 1890, doi:10.5194/gmd–9–1853–2016, 2016.

861   Twomey, S.: The influence of pollution on the shortwave albedo of clouds, J. Atmos. Sci., 34, 1149–1152, 1977.

862   UNEP/WMO: Integrated Assessment of Black Carbon and Tropospheric Ozone, Nairobi, Kenya, available at:

863   http://wedocs.unep.org/handle/20.500.11822/8028 (last access: 13 May 2020), 2011.

864   US EPA: Guidance on the use of models and other analyses for demonstrating attainment of air quality goals for

865   ozone, $PM_{2.5}$, and regional haze. U.S. Environmental Protection Agency Office of Air Quality Planning and

866   Standards Air Quality Analysis Division Air Quality Modeling Group Research Triangle Park, NC, 2007.

867   Zhang, H. Y., Cheng, S. Y., Yao, S., Wang, X. Q., and Zhang, J. F.: Multiple perspectives for modeling regional

868       $PM_{2.5}$ transport across cities in the Beijing–Tianjin–Hebei region during haze episodes, Atmos. Environ., 212,

869   22–35, https://doi.org/10.1016/j.atmosenv.2019.05.031, 2019.

870   Zhang, X., Zhang, Y. H, Han, J. B., Zhang, L., and Shi, W. R.: Analysis of the climatic characteristics of the

871   atmospheric boundary layer height in yanmayan Island, Arctic (in Chinese), Polar studies, 30(02):132–139,

872   2018.